

Article

Solventless Mechanochemical Fabrication of ZnO–MnCO₃/N-Doped Graphene Nanocomposite: Efficacious and Recoverable Catalyst for Selective Aerobic Dehydrogenation of Alcohols under Alkali-Free Conditions

Mujeeb Khan ¹, Syed Farooq Adil ^{1,*}, Mohamed E. Assal ¹, Abdulrahman I. Alharthi ², Mohammed Rafi Shaik ¹, Mufsir Kuniyil ¹, Abdulrahman Al-Warthan ¹, Aslam Khan ³, Zeeshan Nawaz ⁴, Hamid Shaikh ⁵ and Mohammed Rafiq H. Siddiqui ¹

- ¹ Department of Chemistry, College of Science, King Saud University, P.O. Box 2455, Riyadh 11451, Saudi Arabia; kmujeeb@ksu.edu.sa (M.K.); masl@ksu.edu.sa (M.E.A.); mrshaik@ksu.edu.sa (M.R.S.); mkuniyil@ksu.edu.sa (M.K.); awarthan@ksu.edu.sa (A.A.-W.); rafiqs@ksu.edu.sa (M.R.H.S.)
- ² The Department of Chemistry, College of Sciences and Humanities, Prince Sattam Bin Abdulaziz University, P.O. Box 173, Al-Kharj 11942, Saudi Arabia; a.alharthi@psau.edu.sa
- ³ King Abdullah Institute for Nanotechnology, King Saud University, P.O. Box 2454, Riyadh 11451, Saudi Arabia; aslamkhan@ksu.edu.sa
- ⁴ SABIC Technology & Innovation, P.O. Box 5101, Riyadh 11422, Saudi Arabia; zeeshan@sabic.com
- ⁵ SABIC Polymer Research Center (SPRC), Department of Chemical Engineering, King Saud University, P.O. Box 800, Riyadh 11421, Saudi Arabia; hamshaikh@ksu.edu.sa
- * Correspondence: sfadil@ksu.edu.sa; Tel.: +966-11-467-04-39



Citation: Khan, M.; Adil, S.F.; Assal, M.E.; Alharthi, A.I.; Shaik, M.R.; Kuniyil, M.; Al-Warthan, A.; Khan, A.; Nawaz, Z.; Shaikh, H.; et al. Solventless Mechanochemical Fabrication of ZnO–MnCO₃/N-Doped Graphene Nanocomposite: Efficacious and Recoverable Catalyst for Selective Aerobic Dehydrogenation of Alcohols under Alkali-Free Conditions. *Catalysts* **2021**, *11*, 760. <https://doi.org/10.3390/catal11070760>

Academic Editor: Young-Woong Suh

Received: 20 May 2021
Accepted: 17 June 2021
Published: 23 June 2021

Publisher's Note: MDPI stays neutral with regard to jurisdictional claims in published maps and institutional affiliations.



Copyright: © 2021 by the authors. Licensee MDPI, Basel, Switzerland. This article is an open access article distributed under the terms and conditions of the Creative Commons Attribution (CC BY) license (<https://creativecommons.org/licenses/by/4.0/>).

Abstract: Catalytic efficacy of metal-based catalysts can be significantly enhanced by doping graphene or its derivatives in the catalytic protocol. In continuation of previous work regarding the catalytic properties of highly-reduced graphene oxide (HRG), graphene-oxide (GO) doped mixed metal oxide-based nanocomposites, herein we report a simple, straightforward and solventless mechanochemical preparation of N-doped graphene (NDG)/mixed metal oxide-based nanocomposites of ZnO–MnCO₃ (i.e., ZnO–MnCO₃/(X%-NDG)), wherein N-doped graphene (NDG) is employed as a dopant. The nanocomposites were prepared by physical milling of separately fabricated NDG and ZnO–MnCO₃ calcined at 300 °C through eco-friendly ball mill procedure. The as-obtained samples were characterized via X-ray diffraction (XRD), Thermogravimetric analysis (TGA), Fourier-transform infrared spectroscopy (FT-IR), Raman, Field emission scanning electron microscopy (FESEM), Energy-dispersive X-ray spectroscopy (EDX) and surface area analysis techniques. To explore the effectiveness of the obtained materials, liquid-phase dehydrogenation of benzyl alcohol (BOH) to benzaldehyde (BH) was chosen as a benchmark reaction using eco-friendly oxidant (O₂) without adding any harmful surfactants or additives. During the systematic investigation of reaction, it was revealed that the ZnO–MnCO₃/NDG catalyst exhibited very distinct specific-activity (80 mmol/h.g) with a 100% BOH conversion and <99% selectivity towards BH in a very short time. The mechanochemically synthesized NDG-based nanocomposite showed remarkable enhancement in the catalytic performance and increased surface area compared with the catalyst without graphene (i.e., ZnO–MnCO₃). Under the optimum catalytic conditions, the catalyst successfully transformed various aromatic, heterocyclic, allylic, primary, secondary and aliphatic alcohols to their respective ketones and aldehydes with high selectivity and convertibility without over-oxidation to acids. In addition, the ZnO–MnCO₃/NDG was also recycled up to six times with no apparent loss in its efficacy.

Keywords: ZnO nanoparticles; nitrogen doped graphene; nanocomposite; MnCO₃; oxidation; catalyst

1. Introduction

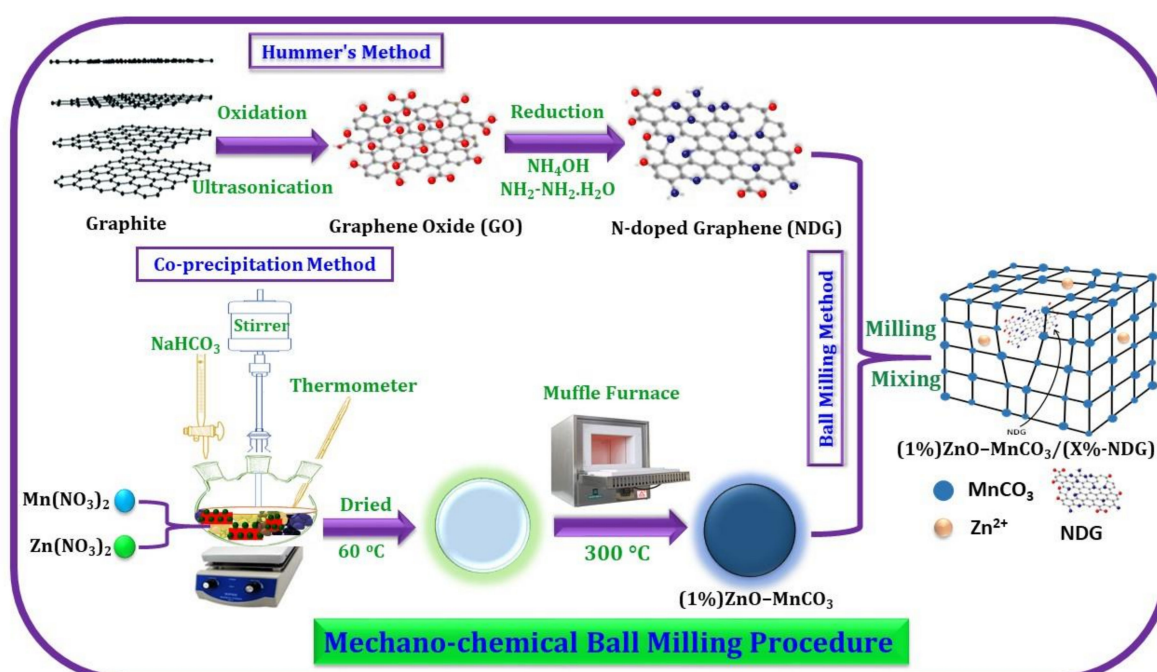
Metal-catalyzed oxidation of alcohols to carbonyls is the most considerable fundamental functional-group reactions in organic synthetic chemistry [1–3]. The oxidative products are essential raw materials and precursors, which have been extensively utilized in the manufacturing of pharmaceuticals, cosmetics, fragrances, dyes, spices, plastics, flame-retardants, insecticides, and agrochemicals [4,5]. In traditional procedures, stoichiometric amounts of inorganic oxidizing agents including KMnO_4 , CrO_3 , NaClO , $\text{Na}_2\text{Cr}_2\text{O}_7$, or PCC were widely used [6,7]. For the most part these oxidants are corrosive, noxious, high cost, toxic and environmentally harmful and demonstrate low selectivity [8]. From the viewpoints of green chemistry and environmental concern, considerable interest has been paid to the design and exploration of ecologically friendly and safer catalytic systems for oxidation of alcohols using greener oxidants like gaseous O_2 [9]. Molecular O_2 possesses various benefits: it is cheap, eco-friendly, abundantly available, and produces clean water as the sole product [10]. In this regard, noble metal catalysts like Au [11], Pd [12], Ru [13], and Pt [14] were extensively applied in the aerial oxygenation of alcohols to carbonyls. However, the high cost and scarceness of these precious metals reduces their industrial applications [15]. Consequently, exploration of plentiful and cheap catalysts like transition (non-noble) metals, such as vanadium- [16], chrome- [17], iron- [18], copper- [19], zirconium- [20], nickel- [21], rhenium- [22], and molybdenum-based catalysts have gained prominence [23] for the selective oxygenation of alcohol. In addition, numerous studies state that the effectiveness of the metal oxide-based catalysts substantially improved after compositing with other metallic NPs, due to the synergistic effects and enhanced surface area [24].

Commonly, metallic and metal oxide NPs are found to be efficacious heterogeneous catalysts for alcohol oxygenation. In addition, the activity of these catalysts could be increased by structure optimization which in-turn increases the specific surface area [25]. However, the nano-sized metal-based catalysts are usually not stable and readily agglomerate owing to huge surface energy, which consequently minimizes their activity and stability [26]. This dilemma can be reduced by suspending these materials on appropriate support which possesses high surface area and prevents particle aggregation [27]. Among various catalysts supports, carbonaceous materials, particularly graphene and its derivatives, like GO, HRG and NDG, have received increasing interest owing to their formidable potential in numerous applications, including catalysis [28]. This is because of the exceptional and unique chemical, physical, electronic, optical and magnetic properties associated with the structural integrity and large surface area of graphene derivatives [29].

Doping of nitrogen has been utilized to fine-tune the structural and electrical properties of graphene, which in-turn leads to significant change of various properties of carbonic materials. Doping creates defects on the surface of the material which offer active anchoring sites to enhance the electronic density and dispersion of catalytically active metal NPs, therefore, this modification will make carbonic materials beneficial in several disciplines [30,31]. The additional N atom on the graphene nano-layer strongly effects the growth-mechanism of NPs, controls the morphology and size of the NPs, as well as assists the uniform dispersion of nanoparticles [32]. In addition, high electro-negativity of N atom also leads to the formation of catalytically active sites, owing to which NDG-based nanocomposites have also been widely utilized as heterogeneous catalysts for plenty of organic transformations [33,34]. Apart from agglomeration of metallic nanoparticles, the inevitable aggregation of graphene nano-layers causes a decrease in its surface areas [32]. Usually, the restacking of graphene nanosheets is prohibited by the inclusion of metals or metal oxides NPs like Pt, Ag, Co_3O_4 , and CeO_2 on the graphene layer [32,35–37]. Indeed, theoretical and experimental studies confirmed the benefits of metals or metal oxides/NDG composites for various catalytic transformations including oxidation of alcohol [38].

Our earlier studies demonstrated the preparation of numerous metal-based nanocatalysts and their graphene nanocomposites and investigated their catalytic performances towards oxidation of alcohols [39–41]. In one such study, we demonstrated the promoting

effect of zinc oxide NPs in the MnCO_3 , i.e., (1%) ZnO-MnCO_3 nanocatalyst which afforded superb activity for aerial dehydrogenation of alcohols in the presence of O_2 . Furthermore, its HRG- and GO-doped catalysts also showed enhanced catalytic activity [40]. In continuation of this work, herein, we prepared (1%) $\text{ZnO-MnCO}_3/(X\%-\text{NDG})$ nanocomposites through a clean and simple two-step process with the co-precipitation method followed by the mechanochemical ball milling (Scheme 1), and investigated their catalytic activity towards aerial dehydrogenation of BOH as a probe reaction. The mechanochemical ball mill procedure helps to decrease the nanoparticles size as well as prohibit aggregation. The fabricated samples were characterized using appropriate microscopic and spectroscopic instruments. The prepared samples were examined for aerial dehydrogenation of a variety of alcohols to investigate the influence of NDG in the resulting nanocomposite. Notably, this is the first study of the catalytic protocol in which NDG-doped ZnO-MnCO_3 is examined for the aerial dehydrogenation of alcohols to carbonyls.



Scheme 1. Synthesis of (1%) $\text{ZnO-MnCO}_3/(X\%-\text{NDG})$ nanocomposites through mechanochemical ball milling technique.

2. Results and Discussion

2.1. Characterizations

XRD analysis was conducted to identify the crystallinity and phases of the as-synthesized materials. Figure 1 reveals the XRD of graphite, GO, NDG, (1%) ZnO-MnCO_3 , and (1%) $\text{ZnO-MnCO}_3/(1\%-\text{NDG})$. The sharp diffraction signal of graphite powder centered at $2\theta = 26.5^\circ$ could be ascribed to the plane (002) with d-spacing of 3.44 Å [42]. Notwithstanding, GO demonstrates a wide band at $2\theta = 11.7^\circ$ which is a fingerprint band for GO structure. The absence of graphite reflection at $2\theta = 26.5^\circ$ and emergence of a novel band at $2\theta = 11.7^\circ$ confirms the successful oxidation of graphite to GO [43]. This 2θ shift is because of the increase in d-spacing from 3.44 to 6.42 Å for graphite and GO, correspondingly, attributed to the existence of residual oxygenic-groups between the graphene nanolayers upon oxidation [44]. XRD diffractogram of pure NDG exhibits a broad band located at approximately $2\theta = 24.5^\circ$ with plane (002) which is a fingerprint band of NDG. The absence of the diffraction band at $2\theta = 11.7^\circ$ confirms the reduction of GO to NDG [45]. XRD diffractogram of undoped catalyst (1%) ZnO-MnCO_3 (without NDG) matches with the rhodochrosite structure of MnCO_3 (JCPDS card no. 1-0981), and the diffraction peaks marked with stars may be ascribed to the existence of

ZnO [46]. For (1%) ZnO–MnCO₃/(1%-NDG) diffractogram, all reflections were assigned to well-crystallized rhodochrosite MnCO₃ structure (JCPDS card no. 1–0981) as well as the fingerprint diffraction band of NDG at approximately 24.5° (as indicated by arrow). Accordingly, the obtained XRD results revealed that the (1%) ZnO–MnCO₃/(1%-NDG) nanocomposite was efficiently synthesized.

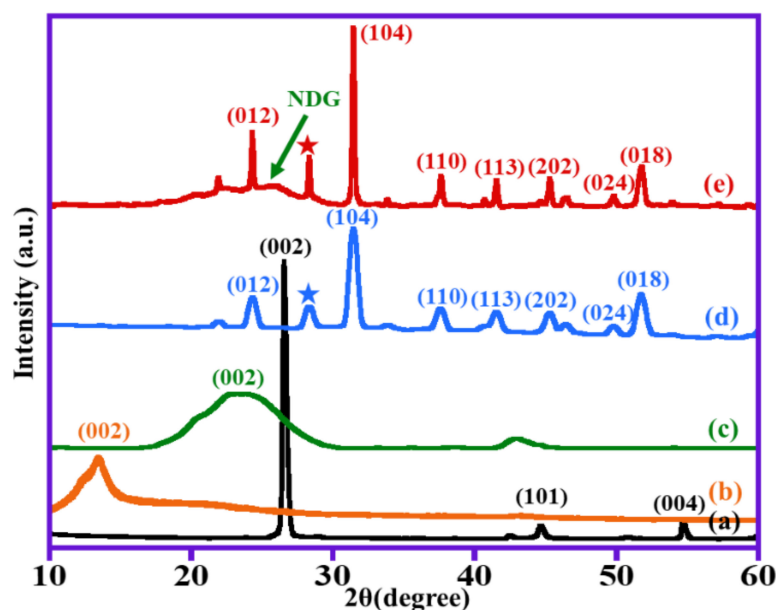


Figure 1. XRD analysis of (a) graphite, (b) GO, (c) NDG, (d) un-doped (1%) ZnO–MnCO₃ catalyst, and (e) (1%)ZnO–MnCO₃/(1%-NDG) samples.

Thermo-gravimetric analyses (TGA) were conducted to determine the thermal property of the fabricated samples up to 800 °C. Figure 2 illustrates the comparison between the thermal stability of (1%) ZnO–MnCO₃/(1%-NDG) nanocomposite and the thermal decomposition properties of its precursors include graphite, GO, NDG, and (1%) ZnO–MnCO₃. The pure graphite powder is highly stable, and displays total weight loss of approximately 1% from 25 °C to 800 °C. It is observed that the pyrolysis of GO is much higher when compared to the graphite, which is ascribed to the existence of labile oxygenated groups on the surface [47]. The GO exhibits ~5% mass loss at 100 °C, attributed to the vaporization of volatile impurities and desorption of water molecules from the structure. The fundamental mass loss of ~44% was observed between 200 and 380 °C because of the thermal degradation of O-carrying groups. Eventually, the mass loss (about 10%) between 380 and 800 °C, related to the pyrolysis of graphene skeleton [48]. However, the NDG thermogram exhibits an entire weight loss of ~30%, which is ascribed to the reduction of oxygenic groups on the surface of graphene. Moreover, the thermogram of (1%) ZnO–MnCO₃/(1%) NDG exhibited a total weight loss of ~19% loss with respect to the 17% weight loss showed by (1%)ZnO–MnCO₃ nanocatalyst over the similar temperature range, which suggests that the doping of the NDG in the nanocomposites slightly depreciates its thermal stability.

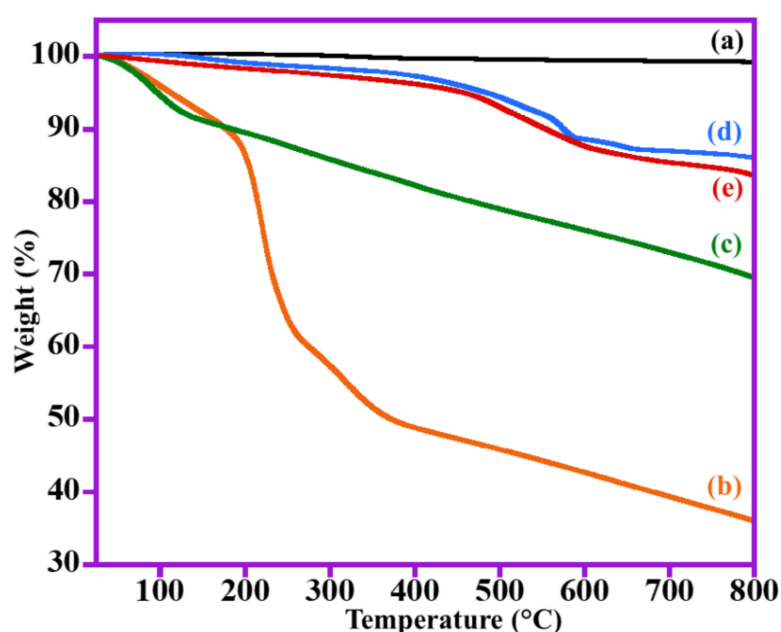


Figure 2. TGA thermogram of (a) graphite, (b) GO, (c) NDG, (d) un-doped (1%) ZnO–MnCO₃ catalyst, and (e) (1%)ZnO–MnCO₃/(1%-NDG) nanocomposite.

FT-IR spectra of the nanocomposite (1%) ZnO–MnCO₃/(1%-NDG) is displayed in Figure 3 and FT-IR results of GO and NDG is also presented for comparison. In pure GO, the band observed at $\sim 3438\text{ cm}^{-1}$ is related to the vibrations of (O–H) bond or physisorbed H₂O molecules [49]. The FT-IR peaks located at 1736 cm^{-1} and 1632 cm^{-1} were assigned to (C=O) vibrational modes and carbon backbone stretching vibrations from un-oxidized graphitic domains, correspondingly [50]. The other absorption peaks observed at 1396 , 1227 , and 1061 cm^{-1} are attributed to vibrations of oxygenic-groups like C–OH, C–O–C (epoxy), and C–O (alkoxy) bonds, correspondingly [51]. The characteristic peaks of oxygenic-functionalities considerably weakened and/or disappeared in the spectrum of pure NDG and (1%) ZnO–MnCO₃/(1%-NDG) nanocomposite, which confirm the effective reduction of GO to NDG. With respect to NDG spectra, some characteristic absorption bands are noticed at 3430 and 1562 cm^{-1} which belong to N–H stretching vibrations and the peak at $\sim 1152\text{ cm}^{-1}$ is associated with C–N [52]. The spectra of (1%) ZnO–MnCO₃/(1%-NDG) exhibits a weak peak at 1634 cm^{-1} due to the vibrations of (C=C) bond, in addition, two strong peaks are present at 865 and 730 cm^{-1} and a wide band exists at 1446 cm^{-1} , which are similar to the peaks that appeared in the IR spectrum of MnCO₃ [53]. Moreover, the broad band at 3430 cm^{-1} is associated with vibrations of N–H and the absorption peak at 1152 cm^{-1} related to (C–N). Lastly, the strong band emerging at 584 cm^{-1} is due to the vibrations of Mn–O bond [54].

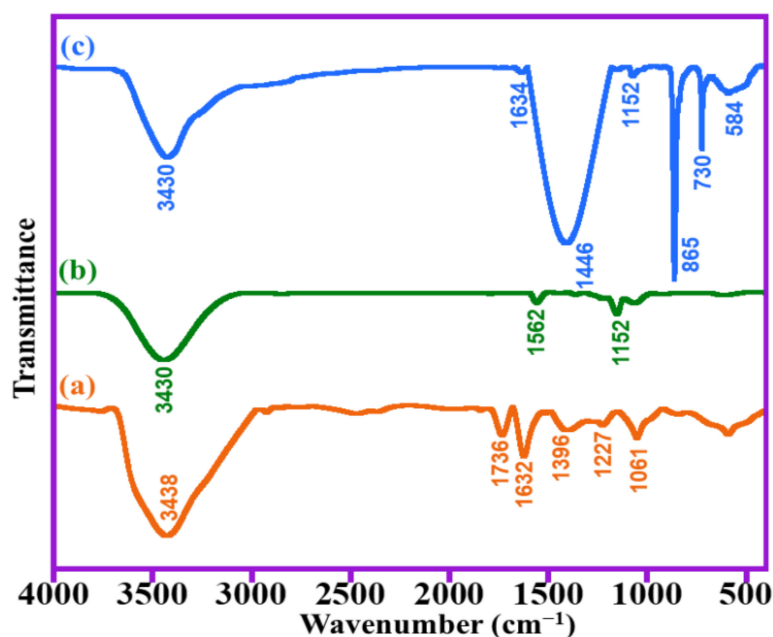


Figure 3. FT-IR results of (a) GO, (b) NDG, and (c) (1%)ZnO–MnCO₃/(1%-NDG).

Raman spectroscopy is an advantageous tool to study the structure of graphite derivatives. Figure 4 illustrates the Raman spectrum of GO, NDG, and (1%) ZnO–MnCO₃/(1%-NDG) nanocomposites. The GO spectrum displays two eminent bands, the G-band at $\sim 1603\text{ cm}^{-1}$ owing to the E_{2g}-phonon of the sp² hybridization carbon atoms, and the D-band at $\sim 1336\text{ cm}^{-1}$ related to the breathing modes of k point phonons of A_{1g}-symmetry. The G-band is usually associated with the well-ordered structure of C–C bond stretching vibrations [55]. The D-band originates from the disorder structure, which could be due to the existence of defects like grain-boundaries, vacancies, and amorphous carbon atoms [56]. Disorder is calculated by the ratio between the intensities of D-band (I_D) and G-band (I_G) i.e., (I_D/I_G). For NDG and (1%) ZnO–MnCO₃/(1%-NDG) spectra, the G-band is located at 1594 cm^{-1} and 1596 cm^{-1} as well as the D-band at 1327 and 1327 cm^{-1} , respectively. The G-band in NDG is red shifted to a lower wavenumber because of the replacing of O atom through N-doping, which leads to the formation of pyrrolic, pyridinic, and N-graphitic instead of sp² carbon atoms [57]. The widened D-band in GO is attributed to the decrease in size of the sp² domains by the creation of defects, distortions, and vacancies upon oxidation. The increment of disorder ratio (I_D/I_G) from 1.088 (GO) to 1.324 (NDG) indicates the incorporation of heterogeneous N atoms into the graphene nanosheets. Eventually, the higher disorder (I_D/I_G) for (1%) ZnO–MnCO₃/(1%-NDG) (1.412), compared to the pure NDG, points to the increasing of defects due to N doping [58].

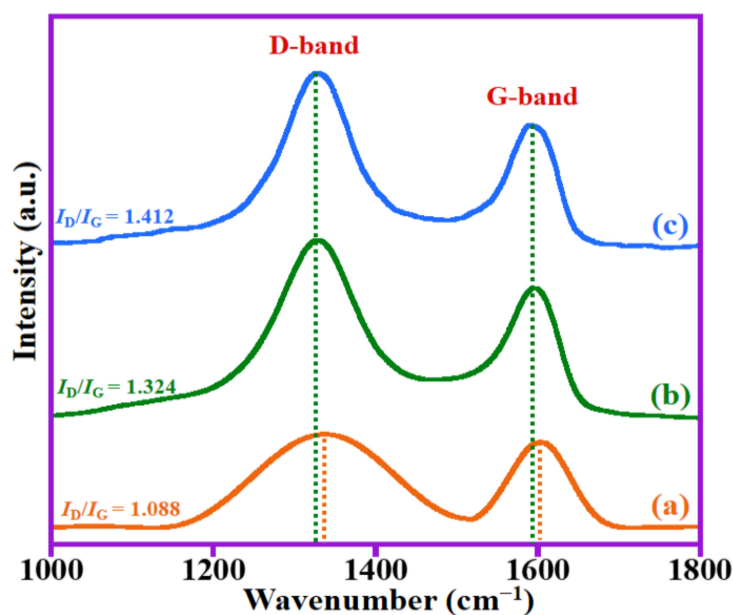


Figure 4. Raman analysis of (a) GO, (b) NDG, and (c) (1%) ZnO–MnCO₃/(1%-NDG).

The sample morphology was examined and the FESEM micrographs of pure NDG, un-doped (1%) ZnO–MnCO₃ catalyst, and (1%) ZnO–MnCO₃/(1%-NDG) nanocomposite is displayed in Figure 5. Figure 5a displays the layer-like structure of NDG as a continual crumpled membrane organized as sheets. The morphology of the un-doped (1%) ZnO–MnCO₃ appears to be rigid and undefined (Figure 5b). Figure 5c,d displays the crumpled NDG layers scattered over a network of NPs. The ZnO–MnCO₃ NPs are with clustered NDG layers over them.

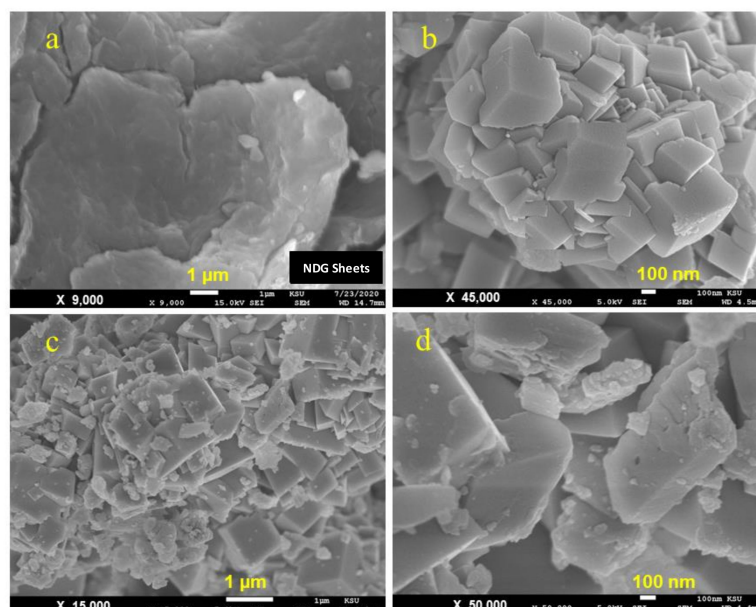


Figure 5. FESEM images of (a) NDG sample, (b) (1%) ZnO–MnCO₃ sample, and (c,d) (1%)ZnO–MnCO₃/(1%-NDG) sample showing presence of NDG sheets.

The elemental mapping of (1%) ZnO–MnCO₃/(1%-NDG) nanocomposite at the rectangular area displayed in Figure 6 discloses the uniform distribution of C (green), Mn (red), O (purple), N (turquoise), and Zn (yellow) atoms throughout the 4 μm sized cross-section. Furthermore, the EDX spectrum of the (1%) ZnO–MnCO₃ sample confirmed the presence

of carbon, oxygen, manganese, and zinc atoms, whereas as expected the EDX spectra of (1%) ZnO–MnCO₃/(1%-NDG) nanocomposite revealed that the existence of carbon, oxygen, manganese, and zinc atoms along with nitrogen atom and the % of N atoms in the nanocomposite is within experimental error to the theoretical composition as demonstrated in Figure 7.

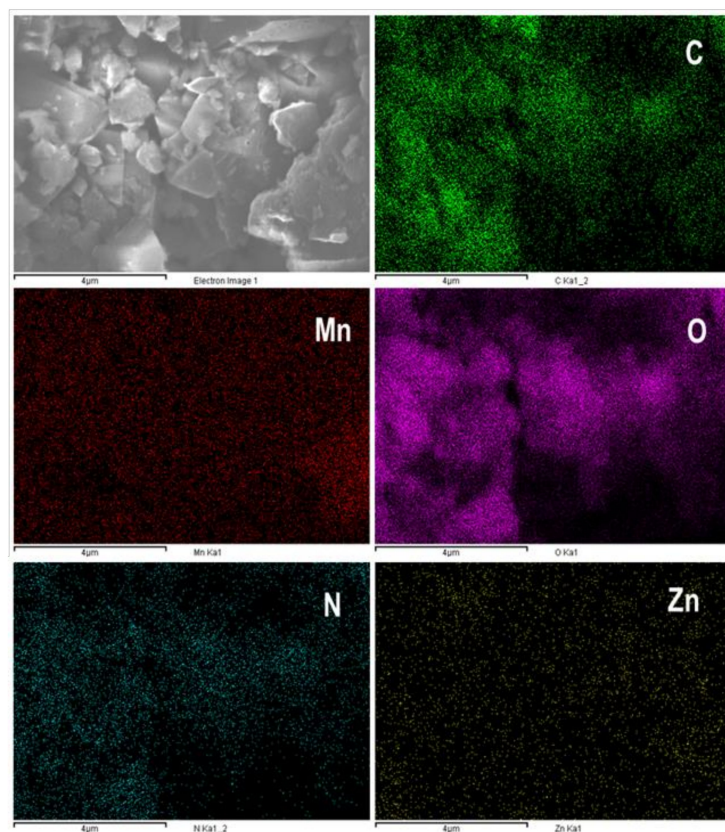


Figure 6. Elemental mapping of (1%) ZnO–MnCO₃/(1%-NDG) nanocomposite.

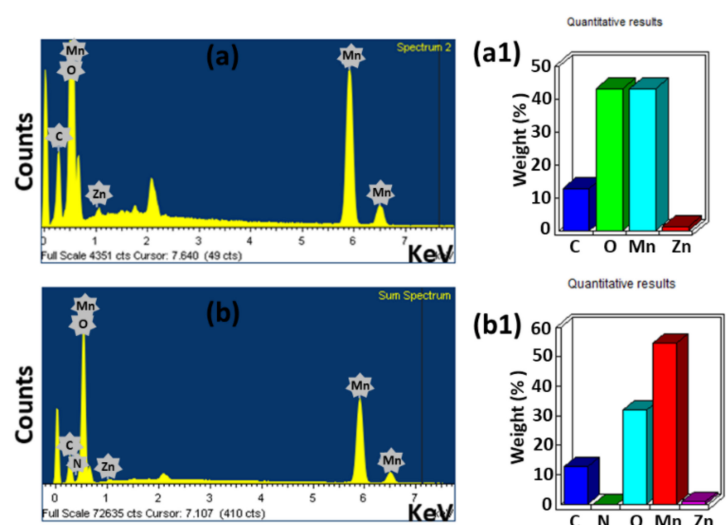


Figure 7. (a) EDX spectra of (1%) ZnO–MnCO₃ sample, (a1) quantitative analysis of (1%)ZnO–MnCO₃ sample, (b) EDX spectra of (1%)ZnO–MnCO₃/(1%-NDG) sample, (b1) quantitative analysis of (1%)ZnO–MnCO₃/(1%-NDG) sample.

To find out the surface areas of the fabricated samples and to comprehend its linkage with the catalytic efficiency for aerobic BOH dehydrogenation, the N_2 sorption mensuration was studied. Table 1 reveals that the surface area of $ZnO-MnCO_3$ (without graphene) is about $120.3\text{ m}^2/\text{g}$. As anticipated, after doping the nanocomposites with graphene supports like HRG, GO, and NDG, the surface areas were considerably raised to 239.1, 244.6, and $261.4\text{ m}^2/\text{g}$, correspondingly.

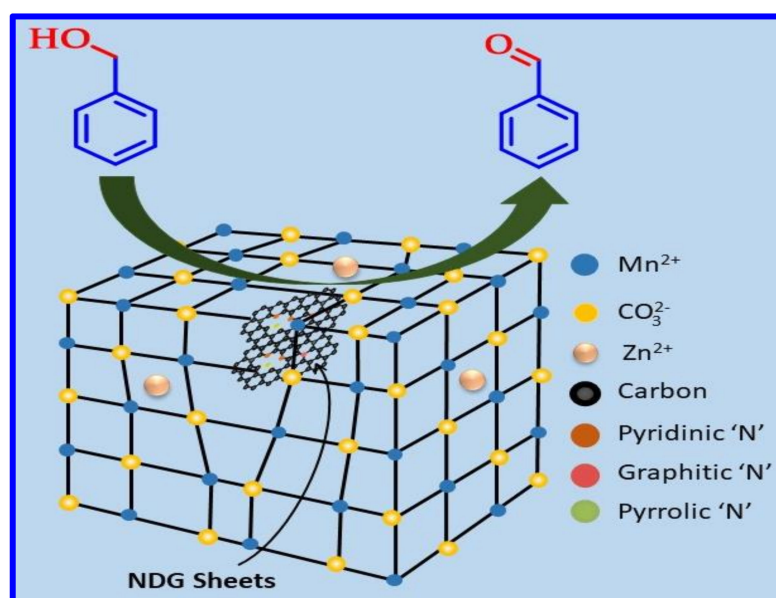
Table 1. Catalytic dehydrogenation of BOH using different prepared catalysts.

E.	Catalyst	Surface Area (m^2/g)	Conv. (%)	Selectivity (%)	Specific-Activity ($\text{mmole}/\text{h.g}$)
1	$MnCO_3$	70.5	38.2	>99	30.6
2	(1%) $ZnO-MnCO_3$	120.3	67.1	>99	53.7
3	(1%) $ZnO-MnCO_3/(1\%-NDG)$	261.4	100.0	>99	80.0
4	(1%) $ZnO-MnCO_3/(1\%-GO)$	244.6	97.8	>99	78.2
5	(1%) $ZnO-MnCO_3/(1\%-HRG)$	239.1	94.9	>99	75.9

Conditions: BOH (2.0 mmole), toluene (15 mL), O_2 flow rate (20 mL/min), catalyst amount (0.30 g), operation temperature (100°C), and time (5 min).

2.2. Catalytic Evaluation Studies

The fundamental objective of this study is to oxidize a variety of alcohols to their respective carbonyl compounds with outstanding catalytic efficacy utilizing O_2 as an environmental-friendly oxidizing agent under alkali-free environment. To achieve this, we utilized NDG as co-dopant for $ZnO-MnCO_3$ nanocatalyst for aerobic dehydrogenation of BOH as a model substrate in the presence of gaseous O_2 , as displayed in Scheme 2. A series of catalysts were prepared by changing the wt. percentage of NDG in the catalytic system. Furthermore, various reaction variables were optimized, such as, catalyst dose, reaction time, and operation temperature, as displayed in Tables 1 and 2 and Figures 8–11.



Scheme 2. Scheme diagram of BOH dehydrogenation in presence of gaseous O_2 catalyzed by the synthesized nanocomposite.

Table 2. Catalytic efficacies of several prepared catalysts.

E.	Catalyst	Conv. (%)	Select. (%)	Specific-Activity (mmole/h.g)
1	NDG	2.4	>99	1.9
2	(1%) ZnO–MnCO ₃	67.1	>99	53.7
3	(1%) ZnO–MnCO ₃ /(1%-NDG)	100.0	>99	80.0
4	(1%) ZnO–MnCO ₃ /(3%-NDG)	92.6	>99	74.1
5	(1%) ZnO–MnCO ₃ /(5%-NDG)	75.5	>99	60.4
6	(1%) ZnO–MnCO ₃ /(7%-NDG)	69.3	>99	55.4

Conditions: BOH (2.0 mmole), toluene (15 mL), O₂ flow rate (20 mL/min), catalyst amount (0.30 g), operation temperature (100 °C), and time (5 min).

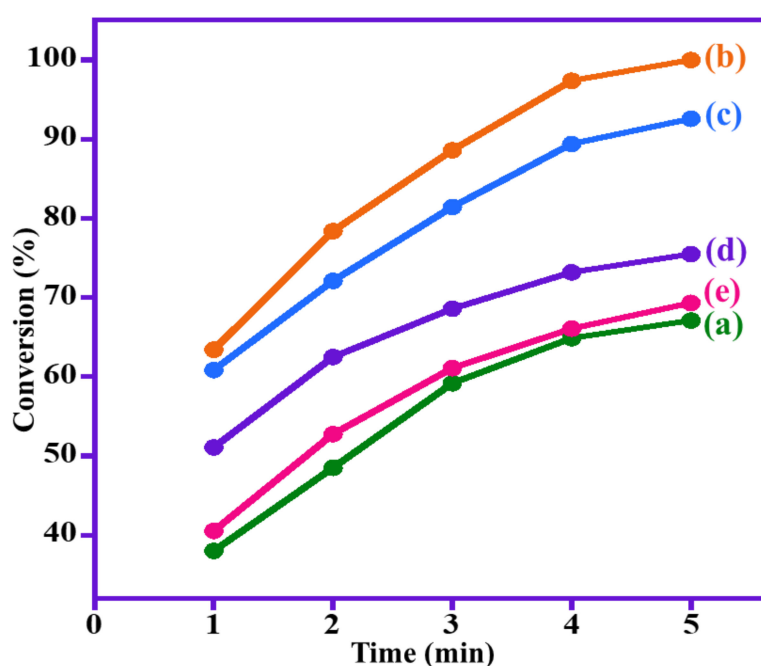


Figure 8. Graphical illustration of BOH dehydrogenation using (a) (1%) ZnO–MnCO₃, (b) (1%) ZnO–MnCO₃/(1%-NDG), (c) (1%) ZnO–MnCO₃/(3%-NDG), (d) (1%) ZnO–MnCO₃/(5%-NDG), and (e) (1%) ZnO–MnCO₃/(7%-NDG) nanocomposites.

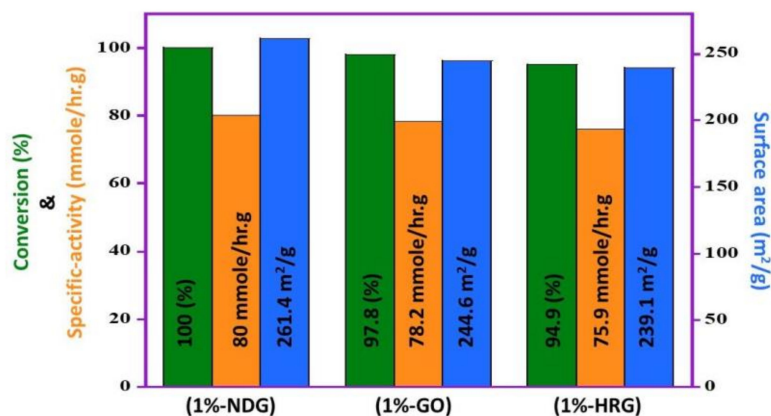


Figure 9. Comparative illustration of effect of various graphene-based dopants in the catalytic system on its catalytic efficiency.

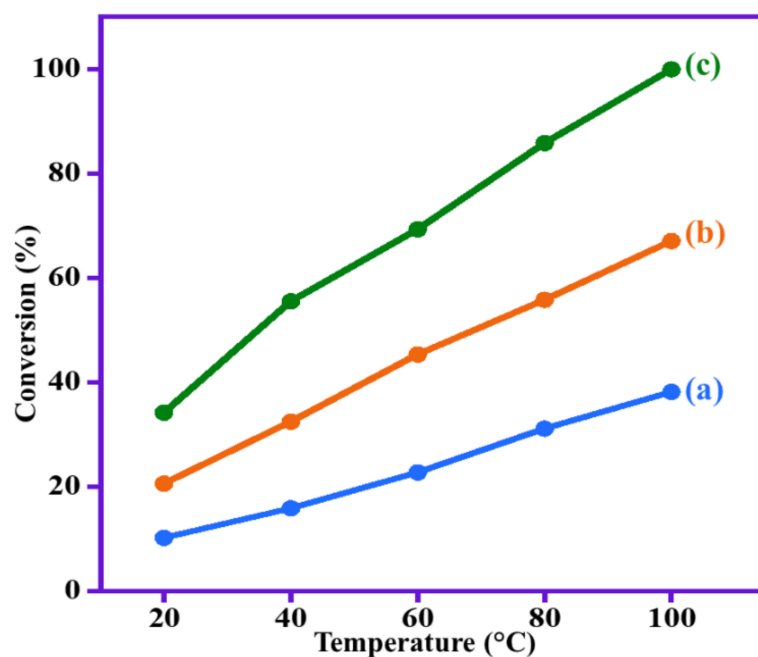


Figure 10. Impact of operation temperature on BOH dehydrogenation using (a) MnCO₃, (b) (1%) ZnO-MnCO₃, and (c) (1%) ZnO-MnCO₃/(1%-NDG).

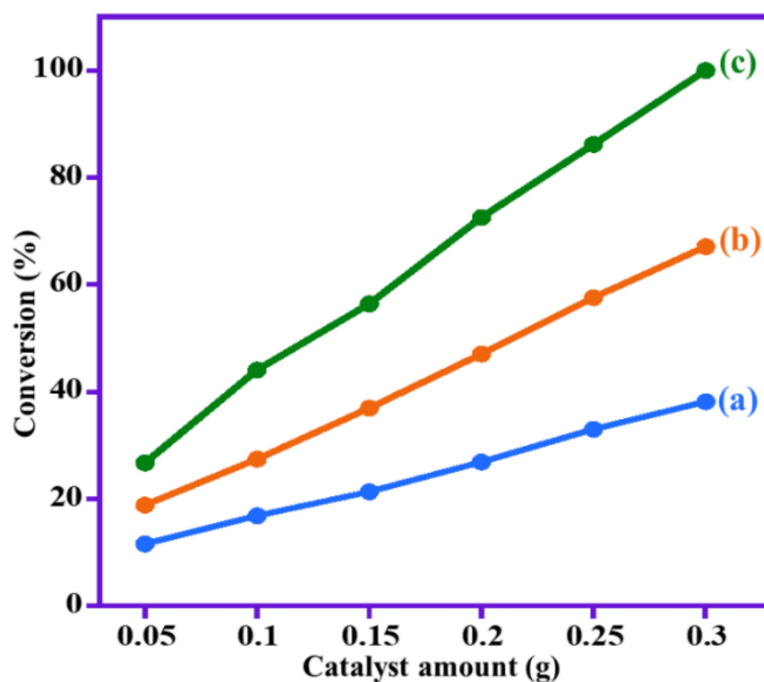


Figure 11. Influence of varying catalyst quantity on BOH oxidation in the presence of (a) MnCO₃, (b) (1%) ZnO-MnCO₃, and (c) (1%) ZnO-MnCO₃/(1%-NDG) catalysts.

2.3. Influence of Weight Percentage of NDG

Commonly, the catalytic ability of the oxidation catalyst remarkably enhanced after employing graphene as a dopant or a supporting material [59,60]. In our previous report, zinc oxide was found to be an ideal dopant for MnCO₃ and (1%) ZnO-MnCO₃ for aerial alcohol dehydrogenation with O₂ as an eco-friendly oxidant. The amount of 0.3 g of (1%) ZnO-MnCO₃ exhibited a full conversion of BOH in 25 min at 100 °C [46]. For this study, (1%) ZnO-MnCO₃ was selected with a purpose of comparing the effects of additional

dopants/support with the earlier catalyst. Notably, initial experiments were devoted to optimizing wt.% of NDG in the nanocomposite to promote the catalytic activity. Firstly, we investigated the efficacy of pristine N-doped graphene towards aerobic dehydrogenation of BOH with gaseous O₂, and its catalytic activity is negligible. However, upon doping as-prepared metal oxide catalysts with varying wt.% of NDG, i.e., (0–7%) NDG, significant catalytic performance was observed towards BOH oxidation as shown in Table 2 and Figure 8. The catalyst without NDG, i.e., (1%) ZnO–MnCO₃, yielded a ~67% conversion of BOH in 5 min. After the addition of 1 wt.% of NDG ((1%) ZnO–MnCO₃/(1%-NDG)), the resulting nanocatalyst displayed enhanced catalytic efficacy. Indeed, the (1%) ZnO–MnCO₃ catalyst with (1%) NDG, i.e., (1%) ZnO–MnCO₃/(1%-NDG), is the best catalyst when compared to other catalysts with different wt.% of NDG. This catalyst yielded 100% conversion within a very short time (5 min) with superb specific-activity of 80 mmole/h.g. Notably, increasing the content of NDG to 3%, a small drop in BOH conversion to ~96% was observed. Similarly, upon further increase of NDG between 5% and 7%, a similar trend was observed and the conversion dropped to ~75% and ~69%, respectively, under the same conditions. It is possible that a higher percentage of NDG may block the active sites of catalyst leading to a decrease in the catalytic activity of the resulting nanocatalyst. Meanwhile, the selectivity towards BH was unaltered during all oxidation processes (>99%). A NMR spectra from one of the reactions depicting the purity of the product formed is given in Supplementary Materials Figure S1. As a result, it can be inferred that NDG played a pivotal role as a dopant in promoting the effectiveness of our catalytic-methodology for this oxidation process.

2.4. Comparison of Various Types of Graphene

Moreover, we compared the effectiveness of (1%) ZnO–MnCO₃ doped with different types of graphene (i.e., GO, HRG, and NDG) for aerobic dehydrogenation of BOH to comprehend the impact of graphene on the efficacy of the catalytic protocol. The data is summed up in Table 1. Firstly, we examined the pristine MnCO₃ (without ZnO NPs) for liquid-phase aerial oxidation of BOH under the above-mentioned circumstances, which only yielded 38.2% BOH conversion within 5 min; however, after doping the MnCO₃ with 1 wt.% of ZnO i.e., (1%) ZnO–MnCO₃, the catalytic performance remarkably increased, and gave 67.1% conversion of BOH at the same experimental conditions. Further modifications were performed by using NDG as a co-dopant, i.e., (1%) ZnO–MnCO₃/(1%-NDG), which has slightly higher activity than the nanocomposites doped with GO ((1%) ZnO–MnCO₃/(1%-GO)) and HRG ((1%) ZnO–MnCO₃/(1%-HRG)). The NDG-doped catalyst yielded 100% conversion, whereas the (1%) ZnO–MnCO₃/(1%-GO) catalyst exhibited 97.8% conversion with specific-activity of 78.2 mmole/h.g. On the other hand, HRG-doped ZnO–MnCO₃ ((1%) ZnO–MnCO₃/(1%-HRG)) exhibited slightly lowered activity when compared to both GO- and NDG-doped catalysts and yielded ~95%. The enhanced efficiency of the NDG-based catalyst can be attributed to the existence of the N atoms on the NDG surface, which increase the electron density of the material [61]. In addition, the existence of NDG could be responsible for extra defects in the crystalline (1%) ZnO–MnCO₃ catalysts which enhance the performance of the nanocomposites. Importantly, the obtained catalytic data of the fabricated catalysts are very much consistent with the Brunauer–Emmett–Teller (BET)-surface area which plays an important role in improving catalytic activity. Interestingly, the catalytic activity after incorporating (1%) ZnO–MnCO₃ with NDG, GO, and HRG, i.e., (1%) ZnO–MnCO₃/(1%-NDG), (1%) ZnO–MnCO₃/(1%-GO), and (1%) ZnO–MnCO₃/(1%-HRG), respectively, also remarkably enhanced. Therefore, it can be said that incorporating graphene derivatives as co-dopants (i.e., NDG, GO, or HRG) had an affirmative effect on the surface area of the as-synthesized nanocomposites, which improves the effectiveness of the catalytic system. Interestingly, the (1%) ZnO–MnCO₃/(1%-NDG) nanocomposite had the highest surface area and also exhibited the best alcohol conversion among all other synthesized graphene-based catalysts, while the other prepared catalysts possessed lower surface area and catalytic efficacy. The comparative graphical illustration of the surface area

and its effect on the catalytic performance is given in Figure 9. Moreover, a comparative graphical illustration of percentage of benzaldehyde (BH) formed using MnCO_3 , ZnO (1%)- MnCO_3 , and their various graphene-based composites is given in Supplementary Materials Figure S2.

2.5. Influence of Temperature

In most cases, the operating temperature plays a pivotal role in catalysis and has a strong impact on the efficacy of catalysts. Subsequently, the effect of temperature on the BOH dehydrogenation was also examined by altering the temperature from RT to 100 °C using the as-prepared catalysts (MnCO_3 , (1%) ZnO-MnCO_3 and (1%) $\text{ZnO-MnCO}_3/(1\%-\text{NDG})$), while maintaining other catalytic variables constant; the data is presented in Figure 10. By increasing the temperature, the catalytic effectiveness also increased, and in all cases superior BH selectivity (>99%) was accomplished. It is noteworthy that the (1%) $\text{ZnO-MnCO}_3/(1\%-\text{NDG})$ catalyst afforded the highest catalytic activity, as illustrated in Figure 10, and moreover, even at RT, the catalyst displayed some conversion (34.2%). Expectedly, higher temperatures lead to higher effectiveness, whereas the optimal temperature with all studied catalysts was found to be 100 °C.

2.6. Influence of Catalyst Dosage

The catalyst quantity optimization tests were conducted by altering the catalyst amount from 0.050 to 0.30 g. Therefore, to study the impact of quantity catalyst (MnCO_3 , (1%) ZnO-MnCO_3 and (1%) $\text{ZnO-MnCO}_3/(1\%-\text{NDG})$), six different amounts (0.05, 0.10, 0.15, 0.20, 0.25 and 0.30 g) were used under similar conditions, and the results are presented in Figure 11. To confirm the importance of catalysts, dehydrogenation was performed in the absence of a catalyst, which did not yield any product. On the other hand, by increasing the catalyst dose from 0.050 to 0.30 g, the conversion also increased significantly, while the BH selectivity remained unchanged throughout all experiments (>99%). Even in all these experiments, (1%) $\text{ZnO-MnCO}_3/(1\%-\text{NDG})$ exhibited maximal efficiency compared to other catalysts. In this case, the percentage conversion improved considerably from 26.7% to 100% upon raising the catalyst dosage from 0.050 to 0.30 g. This can be ascribed to the increased active sites with increasing the amounts of catalysts, which leads to an accelerated oxidation rate.

To exclude the role of solvent (toluene) during oxidation, a blank experiment was performed under optimized conditions without the substrate (BOH) using (1%) $\text{ZnO-MnCO}_3/(1\%-\text{NDG})$ catalyst. No product was obtained, which confirms that the BH is produced only because of the catalytic dehydrogenation of BOH and not toluene. Additionally, to comprehend the significance of the oxidizing agent (O_2) for this transformation, the experiment was performed over the (1%) $\text{ZnO-MnCO}_3/(1\%-\text{NDG})$ employing air instead of bubbling gaseous O_2 . Using the optimal catalytic conditions, the prepared catalyst exhibited only 25.6% alcohol conversion, which is much lower than 100% conversion obtained when this transformation was performed utilizing gaseous O_2 .

2.7. Recycling Tests

Catalyst reutilization has the utmost significance from both an industrial and environmental perspective. Thus, the durability of (1%) $\text{ZnO-MnCO}_3/(1\%-\text{NDG})$ nanocomposite over several usage cycles for aerobic dehydrogenation of BOH with gaseous O_2 was inspected under optimal catalytic circumstances. After carrying out the first experiment, the catalyst was separated by centrifugation. The resulting material was washed with toluene several times and then dried at 105 °C for 3 h. The recovered catalyst was then recycled for this transformation under identical conditions and the conversion of BOH was evaluated using GC. Repeated experiments revealed that the catalyst could be successfully utilized up to six times without compromising its effectiveness. As illustrated in Figure 12, the BOH conversion merely reduced from 100% to ~90% after six runs. The slight reduction in BOH conversion could be due to the slight weight loss of the synthesized sample during

the filtration method [62]. In addition, throughout these reactions, the selectivity towards aldehyde stayed the same (>99%). Therefore, all these results indicate that the (1%) ZnO–MnCO₃/(1%-NDG) has a superb stability as well as reproducibility, which is potentially useful for industrial applications.

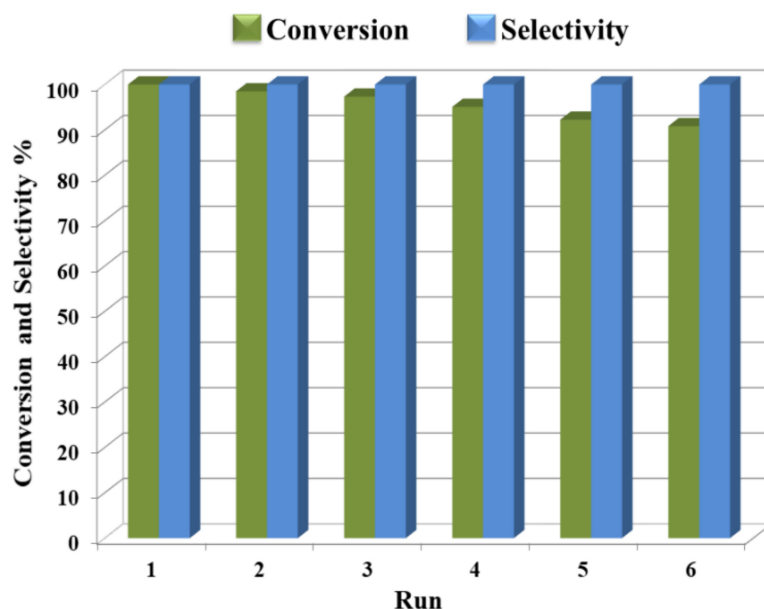


Figure 12. Reusability data of (1%) ZnO–MnCO₃/(1%-NDG) catalyst for aerial dehydrogenation of BOH. Conditions: BOH (2.0 mmole), toluene (15 mL), O₂ flow rate (20 mL/min), catalyst amount (0.30 g), operation temperature (100 °C), and time (5 min).

Moreover, the catalytic activities of nanocatalysts studied herein towards the oxidation of alcohols were compared with similar types of catalytic systems containing GO, HRG, and NDG reported in the literature; the comparison is outlined in Table 3. Compared to the listed catalysts, the (1%) ZnO–MnCO₃/(1%-NDG) demonstrated superior catalytic properties for BOH dehydrogenation with respect to conversion, time, specific-activity, and selectivity. The studied catalyst exhibits 100% transformation of BOH and >99% BH selectivity in a short time with high specific activity, while the other graphene-containing catalysts yielded less conversion, lower specific-activity, and required longer time to complete the reaction. This is possibly ascribed to the presence of a high number of vacancies, distortions, and defects in the NDG, which plays an essential role in improving effectiveness. Xie et al. [63] synthesized Au nanoparticles immobilized in N-doped graphene (AuNPs/NDG) nanocomposite and employed it as an oxidation catalyst for dehydrogenation of BOH. The nanocomposite afforded 67% conversion and 40% selectivity of BH as well as 0.4 mmole/h.g specific-activity within 6 h. Hu and his group [64] reported aerial dehydrogenation of BOH over MnO₂/GO nanocomposite with air as an ecofriendly oxidant with 96.8% conversion of BOH, 100% selectivity of BH, and calculated specific-activity of 1.6 mmole/h.g within 3 h at 110 °C.

2.8. Substrate Scope

Encouraged by the aforementioned observations, we expanded the applicability of the fabricated (1%) ZnO–MnCO₃/(1%-NDG) catalyst for liquid-phase selective dehydrogenation of several kinds of alcohols like primary, secondary, aromatic, aliphatic, allylic, and heterocyclic (Table 4). As demonstrated in Table 4, whole primary benzylic alcohols smoothly oxidize to the respective aldehydes with full conversion in a short time under optimum conditions with no further oxidation to carboxylic acids. Additionally, superb selectivity to corresponding aldehydes or ketones (>99%) was obtained for all alcohols used in this investigation and no other products were detected. The electronic properties of

groups attached to the aromatic alcohols showed a significant influence on the effectiveness due to their capability to give electrons to the benzene ring [65]. It is noteworthy that the electron donating groups have a slightly positive impact on efficacy compared with electron withdrawing substituents; for example, the substituted benzylic alcohol with electron releasing groups like 4-methoxy-benzyl alcohol, was wholly transformed to 4-methoxy-benzaldehyde in 6 min, whereas, 4-trifluoromethyl-benzyl alcohol, that contains an electron withdrawing group, required a longer period (15 min). In addition, aromatic alcohols with substituents at *para*-position were fully transformed after comparatively shorter periods with respect to the *ortho*- and *meta*-positions. This may be due to the minimum steric resistance in *para*-position compared to *ortho*- and *meta*-positions [66].

Table 3. Comparison of the (1%) ZnO–MnCO₃/(1%-NDG) catalyst for aerial oxidation of BOH with already published catalytic systems containing graphene.

Catalyst	Temp. (°C)	Conv. (%)	Select. (%)	Time (h)	Sp. Activity (mmole/h.g)	Ref.
(1%) ZnO–MnCO ₃ /NDG	100	100	<99	0.08	80.0	This study
(1%) ZnO–MnCO ₃ /GO	100	97.8	<99	0.08	78.2	[40]
(1%) ZnO–MnCO ₃ /HRG	100	94.9	<99	0.08	75.9	[39]
AuNPs/NDG	70	67	40	6	0.4	[63]
MnO ₂ /GO	110	96.8	100	3	1.6	[64]
CoO _x /RGO-HP	110	96	<99	6	14.8	[67]
(1%) RGO–MnCoO	140	78	100	2	12.6	[68]
Fe ₃ O ₄ –Pt/rGO	80	33.6	100	3	42.0	[69]
Co/NDG	100	89.5	97.3	8	4.5	[70]
PW@IL-GO	100	94	91	5	12.5	[71]
MnO ₂ –Ag ₂ O/HRG	100	100	<99	0.6	11.4	[72]
GO-100	80	100	100	5	1.1	[73]
Pd NPs/GO	110	36	34.1	6	1.0	[74]
Cu NPs@rGO	80	<99	98.6	16	8.3	[75]
4%Ru(CO)/NDG	90	46	<99	24	6.4	[61]

In this context, *para*-methyl-benzyl alcohol was fully oxidized to *para*-methyl-benzaldehyde in merely 7 min, whilst *ortho*- and *meta*-methyl-benzyl alcohol required relatively longer times such as 15 and 9 min, respectively, for complete conversion. Notably, the steric effect also considerably impacted the rate of oxidation as bulky substrates (2,3,4,5,6-Pentafluoro, 2,4-Dichloro, and 2,3,4-Trimethoxy) attached to an aromatic ring inhibited the efficacy of the oxidation transformation, possibly due to the steric-resistance [71]. Allylic alcohols like cinnamic alcohol also smoothly oxidized to cinnamic aldehyde with 100% conversion and selectivity in 12 min. In addition, a heterocyclic alcohol like furfuryl alcohol was selectively converted to furfural in 28 min, with complete conversion. Furthermore, the present catalysts were also found to be efficient in the dehydrogenation of secondary aromatic alcohols, in which 100% conversion and selectivity towards corresponding ketones was accomplished. Styrallyl alcohol was completely oxidized into acetophenone in just 7 min, while 1-(4-chlorophenyl)ethanol also showed 100% conversion in a relatively longer reaction time (12 min), probably owing to 1-(4-chlorophenyl)ethanol containing an electron withdrawing group that inhibits the benzene ring by minimizing electron density.

Predominantly, by comparing with the dehydrogenation of benzylic alcohols, the aliphatic counterparts are much more difficult under identical conditions [76]. In this regard, the oxidation of cyclohexylmethanol, citronellol, and 1-octanol to their respective aliphatic aldehydes occurs over longer times. Similarly, the dehydrogenation of secondary aliphatic alcohols to aliphatic ketones exhibits lower reactivity with respect to secondary benzylic alcohols. Notably, a longer reaction time could be attributed to the difficulty of dehydrogenation of aliphatic alcohols compared to their aromatic counterparts. Total conversion of styrallyl alcohol occurred in 7 min, whereas the full conversion of 2-octanol

occurred in 140 min. In conclusion, the effectiveness of this catalytic system is significantly affected by the steric and electronic effects.

Table 4. Aerobic base-free dehydrogenation of various alcohols over (1%) ZnO–MnCO₃/(1%-NDG) nanocomposite using gaseous O₂.

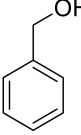
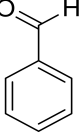
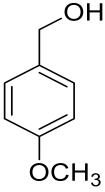
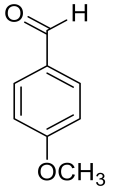
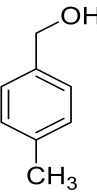
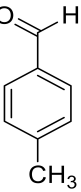
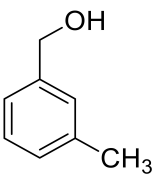
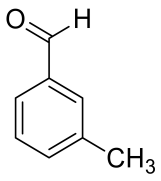
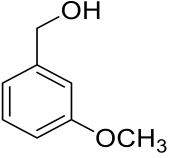
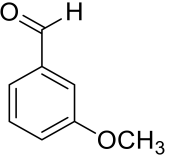
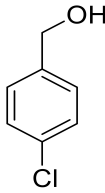
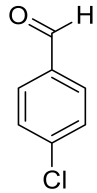
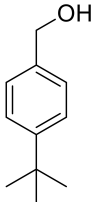
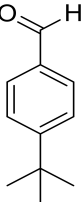
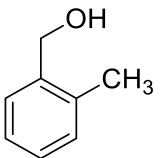
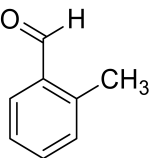
E.	Alcohols	Carbonyl Compounds	Time (minutes)	Conv. (%) / Select. (%)
1			5	100 / >99
2			6	100 / >99
3			7	100 / >99
4			9	100 / >99
5			9	100 / >99
6			10	100 / >99
7			12	100 / >99
8			15	100 / >99

Table 4. Cont.

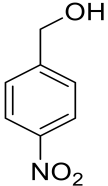
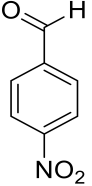
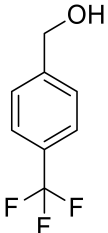
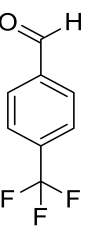
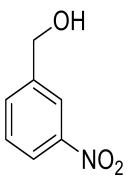
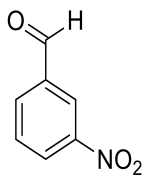
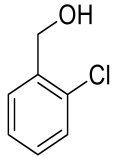
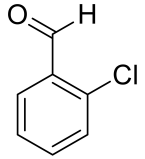
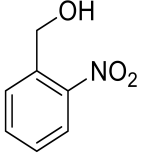
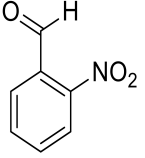
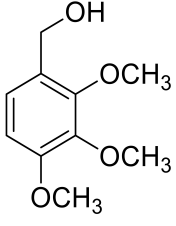
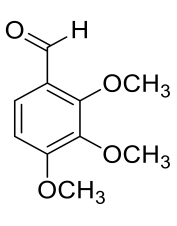
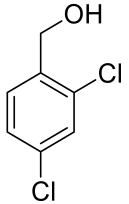
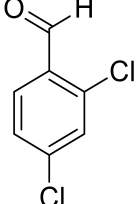
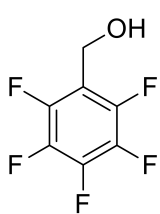
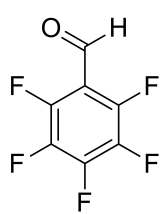
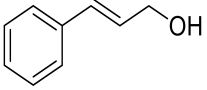
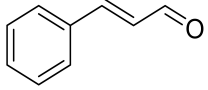
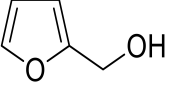
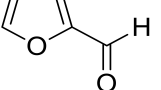
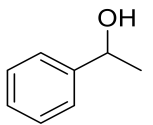
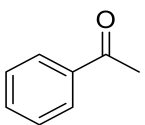
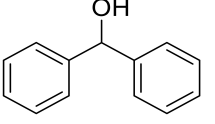
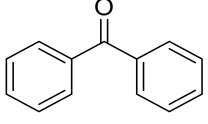
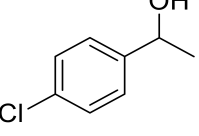
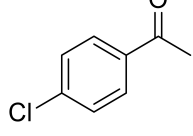
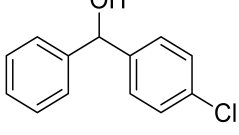
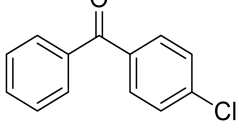
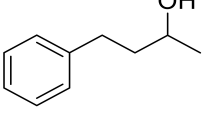
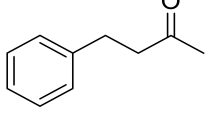
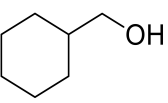
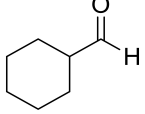
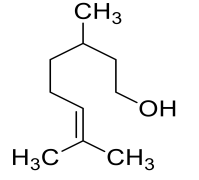
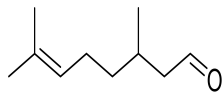
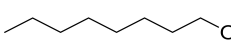
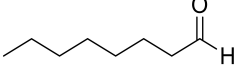
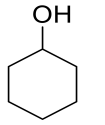
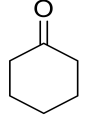
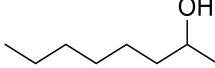
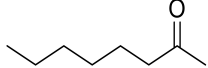
E.	Alcohols	Carbonyl Compounds	Time (minutes)	Conv. (%) / Select. (%)
9			13	100 / >99
10			15	100 / >99
11			18	100 / >99
12			18	100 / >99
13			22	100 / >99
14			22	100 / >99
15			25	100 / >99
16			30	100 / >99

Table 4. Cont.

E.	Alcohols	Carbonyl Compounds	Time (minutes)	Conv. (%) / Select. (%)
17			12	100 / >99
18			28	100 / >99
19			7	100 / >99
20			9	100 / >99
21			12	100 / >99
22			15	100 / >99
23			25	100 / >99
24			40	100 / >99
25			125	100 / >99
26			135	100 / >99
27			45	100 / >99
28			140	100 / >99

Conditions: Substrate (2.0 mmole), (1%) ZnO–MnCO₃ / (1%-NDG) catalyst annealed at 300 °C (0.30 g), toluene (10 mL), O₂ flow rate (20 mL/min), operation temperature (100 °C), and time (5 min).

3. Experimental Part

3.1. Preparation of GO and NDG

GO was fabricated from graphite using Hummers oxidation route [77], thereafter, GO was reduced and doped by using NH_4OH and $\text{NH}_2\text{NH}_2 \cdot \text{H}_2\text{O}$ to obtain N-doped graphene for which the experimental details are mentioned in the Supplementary File.

3.2. Preparation of (1%) ZnO-MnCO_3 /(X%-NDG)

Briefly, ZnO NPs-MnCO_3 were synthesized by coprecipitation procedure by mixing stoichiometric concentrations of $\text{Zn}(\text{NO}_3)_2$ and $\text{Mn}(\text{NO}_3)_2$ solutions in a round-bottomed flask and the mixture was continuously stirred at 96°C . The solution of NaHCO_3 (0.50 M) was added drop-wise to the solution until the pH reached ~ 9 , then the addition was stopped and the reaction mixture was stirred at the same temperature for 4 h. Vigorous stirring was continued overnight at RT. The resulting solution was filtered and then dried at 65°C overnight. The resultant powder sample was calcined at 300°C in a muffle-furnace and ZnO NPs-MnCO_3 was obtained. Subsequently, the synthesized NDG was dried in a furnace at 65°C and firstly ground in a planetary ball mill. Then varied weight percentages of NDG were mixed with (1%) ZnO-MnCO_3 in a planetary ball mill to get (1%) ZnO-MnCO_3 doped (X%-NDG) nanocomposites (i.e., (1%) ZnO-MnCO_3 /(X%-NDG)). The details related to the planetary ball mill method are given in the Supplementary Information.

3.3. Characterizations

The synthesized samples were characterized utilizing several techniques. Specifics about instruments are described in the Supplementary File.

3.4. Catalytic Evaluation Tests

The typical process for aerobic base-free dehydrogenation of alcohols is mentioned in the Supplementary Information.

4. Conclusions

Herein, ZnO nanoparticles doped MnCO_3 co-doped with nitrogen-doped graphene (NDG) nanocomposites were prepared via a co-precipitation procedure followed by a mechanochemical procedure. The fabricated nanocomposites were employed for aerial alkali-free dehydrogenation of BOH with gaseous O_2 as an environmentally friendly oxidant. The efficacies of (1%) ZnO-MnCO_3 doped with different graphene derivatives (NDG, GO, and HRG) were compared for this transformation to understand the role of different graphene derivatives in this catalytic system. The results disclosed that the (1%) ZnO-MnCO_3 /NDG has higher catalytic activity than undoped catalyst (1%) ZnO-MnCO_3 , (1%) ZnO-MnCO_3 /GO, and (1%) ZnO-MnCO_3 /HRG. The higher effectiveness of (1%) ZnO-MnCO_3 /(1%-NDG) could be ascribed to the presence of NDG, which influences the interactions between N-atoms on the surface of NDG and (1%) ZnO-MnCO_3 NPs. Furthermore, the presence of graphene layers develops numerous defects and distortions in structure, which facilitate the adsorption of aromatic reactants at catalytically active sites which promote the interactions between NDG surface and acidic substrates, leading to enhanced catalytic activities. The best results were achieved in the case of (1%) ZnO-MnCO_3 /(1%-NDG) catalyst which led to a 100% BOH conversion and >99% product selectivity in quite a short time. The catalyst also delivered excellent specific activity (80 mmole/h.g) when compared to published studies. Notably, the dehydrogenation of aromatic alcohols is much easier than aliphatic ones, presumably because of the strong π - π stacking interactions between aromatic substrates and graphene sheets. The (1%) ZnO-MnCO_3 /(1%-NDG) catalyst can be reused efficiently without compromising its activity up to six times. The main features of the studied catalytic system are: (a) simple workup, (b) easily available precursors, (c) low cost and green oxidant, (d) no external additives or nitrogenous alkalis, (e) mild reaction conditions, (f) inexpensive recyclable catalyst, (g)

highly efficient in case of both conversion and selectivity, (h) shorter reaction time, and (i) effective for all kinds of alcohols.

Supplementary Materials: The following are available online at <https://www.mdpi.com/article/10.3390/catal11070760/s1>. Figure S1. ¹H NMR spectra for the product (benzaldehyde) obtained after selective oxidation of benzyl alcohol; Figure S2. Comparative graphical illustration of percentage of benzaldehyde (BH) formed using MnCO₃, ZnO(1%)-MnCO₃ and their various graphene based composites within 5 minutes.

Author Contributions: M.K. (Mujeb Khan): formal analysis; investigation; writing—review and editing; S.F.A.: conceptualization; investigation; methodology; writing—original draft; writing—review and editing; M.E.A.: formal analysis; investigation; writing—original draft; A.I.A.: formal analysis; M.R.S.: formal analysis; investigation; M.K. (Mufsir Kuniyil): formal analysis; investigation; A.A.-W.: supervision; A.K.: formal analysis; Z.N.: formal analysis; H.S.: formal analysis; M.R.H.S.: supervision. All authors have read and agreed to the published version of the manuscript.

Funding: The authors extend their appreciation to the Deanship of Scientific Research at King Saud University for funding this work through Research Group No. RG-1436-032.

Data Availability Statement: The data contained within the article and supplementary file.

Acknowledgments: The authors extend their appreciation to the Deanship of Scientific Research at King Saud University for funding this work through Research Group No. RG-1436-032.

Conflicts of Interest: The authors declare no conflict of interest.

References

1. Taghavimoghaddam, J.; Knowles, G.P.; Chaffee, A.L. Preparation and Characterization of Mesoporous Silica Supported Cobalt Oxide as a Catalyst for the Oxidation of Cyclohexanol. *J. Mol. Catal. A Chem.* **2012**, *358*, 79–88.
2. Karimi, B.; Rostami, F.B.; Khorasani, M.; Elhamifar, D.; Vali, H. Selective Oxidation of Alcohols with Hydrogen Peroxide Catalyzed by Tungstate Ions (WO₄[−]) Supported on Periodic Mesoporous Organosilica with Imidazolium Frameworks (PMO-IL). *Tetrahedron* **2014**, *70*, 6114–6119.
3. Marella, R.K.; Neeli, C.K.P.; Kamaraju, S.R.R.; Burri, D.R. Highly active Cu/MgO catalysts for selective dehydrogenation of benzyl alcohol into benzaldehyde using neither O₂ nor H₂ acceptor. *Catal. Sci. Technol.* **2012**, *2*, 1833–1838.
4. Du, Z.; Ma, J.; Ma, H.; Gao, J.; Xu, J. Synergistic effect of vanadium–phosphorus promoted oxidation of benzylic alcohols with molecular oxygen in water. *Green Chem.* **2010**, *12*, 590–592.
5. Kantam, M.L.; Reddy, R.S.; Pal, U.; Sudhakar, M.; Venugopal, A.; Ratnam, K.J.; Figueras, F.; Chintareddy, V.R.; Nishina, Y. Ruthenium/magnesium–lanthanum mixed oxide: An efficient reusable catalyst for oxidation of alcohols by using molecular oxygen. *J. Mol. Catal. A Chem.* **2012**, *359*, 1–7.
6. Tonucci, L.; Nicastro, M.; d’Alessandro, N.; Bressan, M.; D’Ambrosio, P.; Morvillo, A. Catalytic Aerobic Oxidation of Allylic Alcohols to Carbonyl Compounds under Mild Conditions. *Green Chem.* **2009**, *11*, 816–820.
7. Zhan, G.; Hong, Y.; Mbah, V.T.; Huang, J.; Ibrahim, A.-R.; Du, M.; Li, Q. Bimetallic Au–Pd/MgO as efficient catalysts for aerobic oxidation of benzyl alcohol: A green bio-reducing preparation method. *Appl. Catal. A* **2012**, *439*, 179–186.
8. Enache, D.I.; Edwards, J.K.; Landon, P.; Solsona-Espriu, B.; Carley, A.F.; Herzing, A.A.; Watanabe, M.; Kiely, C.J.; Knight, D.W.; Hutchings, G.J. Solvent-Free Oxidation of Primary Alcohols to Aldehydes Using Au–Pd/TiO₂ Catalysts. *Science* **2006**, *311*, 362–365.
9. Parmeggiani, C.; Cardona, F. Transition metal based catalysts in the aerobic oxidation of alcohols. *Green Chem.* **2012**, *14*, 547–564.
10. Dell’Anna, M.M.; Mali, M.; Mastroilli, P.; Cotugno, P.; Monopoli, A. Oxidation of Benzyl Alcohols to Aldehydes and Ketones under Air in Water Using a Polymer Supported Palladium Catalyst. *J. Mol. Catal. A Chem.* **2014**, *386*, 114–119.
11. Adnan, R.H.; Andersson, G.G.; Polson, M.I.; Metha, G.F.; Golovko, V.B. Factors Influencing the Catalytic Oxidation of Benzyl Alcohol Using Supported Phosphine-Capped Gold Nanoparticles. *Catal. Sci. Technol.* **2015**, *5*, 1323–1333.
12. Liu, K.; Yan, X.; Zou, P.; Wang, Y.; Dai, L. Large Size Pd Nps Loaded on TiO₂ as Efficient Catalyst for the Aerobic Oxidation of Alcohols to Aldehydes. *Catal. Commun.* **2015**, *58*, 132–136.
13. Csajernyk, G.; Éll, A.H.; Fadini, L.; Pugin, B.; Bäckvall, J.-E. Efficient Ruthenium-Catalyzed Aerobic Oxidation of Alcohols Using a Biomimetic Coupled Catalytic System. *J. Org. Chem.* **2002**, *67*, 1657–1662.
14. Li, Y.; Bian, T.; Du, J.; Xiong, Y.; Zhan, F.; Zhang, H.; Yang, D. Facile Synthesis of High-Quality Pt Nanostructures with a Controlled Aspect Ratio for Methanol Electro-Oxidation. *CrystEngComm* **2014**, *16*, 8340–8343.
15. Tanaka, K.; Shoji, T.; Hirano, M. Cationic Rhodium (I)/Bisphosphane Complex-Catalyzed Isomerization of Secondary Propargylic Alcohols to α , β -Enones. *Eur. J. Org. Chem.* **2007**, *2007*, 2687–2699.
16. Behera, G.C.; Parida, K. Liquid Phase Catalytic Oxidation of Benzyl Alcohol to Benzaldehyde over Vanadium Phosphate Catalyst. *Appl. Catal. A* **2012**, *413*, 245–253.

17. Noshiranzadeh, N.; Bikas, R.; Ślepokura, K.; Mayeli, M.; Lis, T. Synthesis, characterization and catalytic activity of new Cr (III) complex in oxidation of primary alcohols to aldehydes. *Inorg. Chim. Acta* **2014**, *421*, 176–182.
18. Cang, R.; Lu, B.; Li, X.; Niu, R.; Zhao, J.; Cai, Q. Iron-chloride ionic liquid immobilized on SBA-15 for solvent-free oxidation of benzyl alcohol to benzaldehyde with H_2O_2 . *Chem. Eng. Sci.* **2015**, *137*, 268–275.
19. Cruz, P.; Pérez, Y.; del Hierro, I.; Fajardo, M. Copper, copper oxide nanoparticles and copper complexes supported on mesoporous SBA-15 as catalysts in the selective oxidation of benzyl alcohol in aqueous phase. *Microporous Mesoporous Mater.* **2016**, *220*, 136–147.
20. Goh, T.W.; Xiao, C.; Maligal-Ganesh, R.V.; Li, X.; Huang, W. Utilizing mixed-linker zirconium based metal-organic frameworks to enhance the visible light photocatalytic oxidation of alcohol. *Chem. Eng. Sci.* **2015**, *124*, 45–51.
21. Kawabata, T.; Shinozuka, Y.; Ohishi, Y.; Shishido, T.; Takaki, K.; Takehira, K. Nickel containing Mg-Al hydrotalcite-type anionic clay catalyst for the oxidation of alcohols with molecular oxygen. *J. Mol. Catal. A Chem.* **2005**, *236*, 206–215.
22. Sousa, S.C.; Bernardo, J.R.; Florindo, P.R.; Fernandes, A.C. Efficient and selective oxidation of alcohols catalyzed by oxo-rhenium complexes. *Catal. Commun.* **2013**, *40*, 134–138.
23. Rao, P.S.N.; Rao, K.T.V.; Prasad, P.S.S.; Lingaiah, N. The Role of Vanadia for the Selective Oxidation of Benzyl Alcohol over Heteropolymolybdate Supported on Alumina. *Chin. J. Catal.* **2011**, *32*, 1719–1726.
24. Arena, F.; Gumina, B.; Lombardo, A.F.; Espro, C.; Patti, A.; Spadaro, L.; Spiccia, L. Nanostructured MnO_x Catalysts in the Liquid Phase Selective Oxidation of Benzyl Alcohol with Oxygen: Part I. Effects of Ce and Fe Addition on Structure and Reactivity. *Appl. Catal. B Environ.* **2015**, *162*, 260–267.
25. Assal, M.E.; Kuniyil, M.; Khan, M.; Shaik, M.R.; Al-Warthan, A.; Siddiqui, M.R.H.; Labis, J.P.; Adil, S.F. Comparative Catalytic Evaluation of Nano-ZrO_x Promoted Manganese Catalysts: Kinetic Study and the Effect of Dopant on the Aerobic Oxidation of Secondary Alcohols. *Adv. Mater. Sci. Eng.* **2017**, *2017*, 1–14.
26. Liu, Y.; Zhang, J.; Guan, H.; Zhao, Y.; Yang, J.-H.; Zhang, B. Preparation of bimetallic Cu-Co nanocatalysts on poly (diallyldimethylammonium chloride) functionalized halloysite nanotubes for hydrolytic dehydrogenation of ammonia borane. *Appl. Surf. Sci.* **2018**, *427*, 106–113.
27. Shinde, V.M.; Skupien, E.; Makkee, M. Synthesis of highly dispersed Pd nanoparticles supported on multi-walled carbon nanotubes and their excellent catalytic performance for oxidation of benzyl alcohol. *Catal. Sci. Tech.* **2015**, *5*, 4144–4153.
28. Khan, M.; Tahir, M.N.; Adil, S.F.; Khan, H.U.; Siddiqui, M.R.H.; Al-warthan, A.A.; Tremel, W. Graphene based metal and metal oxide nanocomposites: Synthesis, properties and their applications. *J. Mater. Chem. A* **2015**, *3*, 18753–18808.
29. Zhu, S.; Wang, J.; Fan, W. Graphene-based catalysis for biomass conversion. *Catal. Sci. Technol.* **2015**, *5*, 3845–3858.
30. Guan, H.; Liu, Y.; Bai, Z.; Zhang, J.; Yuan, S.; Zhang, B. Ag nanoparticles embedded in N-doped carbon nanofibers: A superior electrocatalyst for hydrogen peroxide detection. *Mater. Chem. Phys.* **2018**, *213*, 335–342.
31. Jia, Z.; Huang, F.; Diao, J.; Zhang, J.; Wang, J.; Su, D.S.; Liu, H. Pt NPs immobilized on a N-doped graphene@ Al_2O_3 hybrid support as robust catalysts for low temperature CO oxidation. *Chem. Commun.* **2018**, *54*, 11168–11171.
32. Wang, X.; Li, X.; Liu, D.; Song, S.; Zhang, H. Green synthesis of Pt/CeO₂/graphene hybrid nanomaterials with remarkably enhanced electrocatalytic properties. *Chem. Commun.* **2012**, *48*, 2885–2887.
33. Qiao, X.; Liao, S.; You, C.; Chen, R. Phosphorus and nitrogen dual doped and simultaneously reduced graphene oxide with high surface area as efficient metal-free electrocatalyst for oxygen reduction. *Catalysts* **2015**, *5*, 981–991.
34. Jeon, I.Y.; Zhang, S.; Zhang, L.; Choi, H.J.; Seo, J.M.; Xia, Z.; Dai, L.; Baek, J.B. Edge-selectively sulfurized graphene nanoplatelets as efficient metal-free electrocatalysts for oxygen reduction reaction: The electron spin effect. *Adv. Mater.* **2013**, *25*, 6138–6145.
35. Ji, Z.; Shen, X.; Yang, J.; Zhu, G.; Chen, K. A novel reduced graphene oxide/Ag/CeO₂ ternary nanocomposite: Green synthesis and catalytic properties. *Appl. Catal. B.* **2014**, *144*, 454–461.
36. Li, Y.; Gao, W.; Ci, L.; Wang, C.; Ajayan, P.M. Catalytic performance of Pt nanoparticles on reduced graphene oxide for methanol electro-oxidation. *Carbon* **2010**, *48*, 1124–1130.
37. Wu, Z.-S.; Ren, W.; Wen, L.; Gao, L.; Zhao, J.; Chen, Z.; Zhou, G.; Li, F.; Cheng, H.-M. Graphene anchored with Co₃O₄ nanoparticles as anode of lithium ion batteries with enhanced reversible capacity and cyclic performance. *ACS Nano* **2010**, *4*, 3187–3194.
38. Rao, R.; Sun, H.; Dong, X.; Dong, H.; Fang, W.; Tang, Y.; Fang, S.; Hu, C. A facile and large-scale synthesis of Co₃O₄/N-doped graphene for CO oxidation: Low-temperature catalytic activity and the role of nitrogen states. *Appl. Surf. Sci.* **2020**, *513*, 145800.
39. Assal, M.E.; Shaik, M.R.; Kuniyil, M.; Khan, M.; Alzahrani, A.Y.; Al-Warthan, A.; Siddiqui, M.R.H.; Adil, S.F. Mixed Zinc/Manganese on Highly Reduced Graphene Oxide: A Highly Active Nanocomposite Catalyst for Aerial Oxidation of Benzylic Alcohols. *Catalysts* **2017**, *7*, 391.
40. Adil, S.F.; Assal, M.E.; Shaik, M.R.; Kuniyil, M.; Hashmi, A.; Khan, M.; Khan, A.; Tahir, M.N.; Al-Warthan, A.; Siddiqui, M.R.H. Efficient aerial oxidation of different types of alcohols using ZnO nanoparticle–MnCO₃–graphene oxide composites. *Appl. Organomet. Chem.* **2020**, *34*, e5718.
41. Adil, S.F.; Assal, M.E.; Shaik, M.R.; Kuniyil, M.; Alotaibi, N.M.; Khan, M.; Sharif, M.; Alam, M.M.; Al-Warthan, A.; Mohammed, J.A.; et al. A Facile Synthesis of ZrO_x–MnCO₃/Graphene Oxide (GRO) Nanocomposites for the Oxidation of Alcohols using Molecular Oxygen under Base Free Conditions. *Catalysts* **2019**, *9*, 759.
42. Wang, H.; Hu, Y.H. Effect of Oxygen Content on Structures of Graphite Oxides. *Ind. Eng. Chem. Res.* **2011**, *50*, 6132–6137.
43. Yang, S.; Lin, Y.; Song, X.; Zhang, P.; Gao, L. Covalently Coupled Ultrafine H-TiO₂ Nanocrystals/Nitrogen-Doped Graphene Hybrid Materials for High-Performance Supercapacitor. *ACS Appl. Mater. Interfaces* **2015**, *7*, 17884–17892.

44. Zhang, S.; Zhu, L.; Song, H.; Chen, X.; Wu, B.; Zhou, J.; Wang, F. How graphene is exfoliated from graphitic materials: Synergistic effect of oxidation and intercalation processes in open, semi-closed, and closed carbon systems. *J. Mater. Chem.* **2012**, *22*, 22150–22154.
45. Hu, Z.; Zhou, G.; Xu, L.; Yang, J.; Zhang, B.; Xiang, X. Preparation of ternary Pd/CeO₂-nitrogen doped graphene composites as recyclable catalysts for solvent-free aerobic oxidation of benzyl alcohol. *Appl. Surf. Sci.* **2019**, *471*, 852–861.
46. Adil, S.F.; Assal, M.E.; Kuniyil, M.; Khan, M.; Shaik, M.R.; Alwarthan, A.; Labis, J.P.; Siddiqui, M.R.H. Synthesis and comparative catalytic study of zinc oxide (ZnO_x) nanoparticles promoted MnCO₃, MnO₂ and Mn₂O₃ for selective oxidation of benzylic alcohols using molecular oxygen. *Mater. Express* **2017**, *7*, 79–92.
47. Wang, Z.-L.; Xu, D.; Huang, Y.; Wu, Z.; Wang, L.-M.; Zhang, X.-B. Facile, mild and fast thermal-decomposition reduction of graphene oxide in air and its application in high-performance lithium batteries. *Chem. Commun.* **2012**, *48*, 976–978.
48. Lerf, A.; He, H.; Forster, M.; Klinowski, J. Structure of graphite oxide revisited. *J. Phys. Chem. B* **1998**, *102*, 4477–4482.
49. Wang, Y.; Zhao, Y.; He, W.; Yin, J.; Su, Y. Palladium nanoparticles supported on reduced graphene oxide: Facile synthesis and highly efficient electrocatalytic performance for methanol oxidation. *Thin Solid Film.* **2013**, *544*, 88–92.
50. Sitko, R.; Turek, E.; Zawisza, B.; Malicka, E.; Talik, E.; Heimann, J.; Gabor, A.; Feist, B.; Wrzalik, R. Adsorption of divalent metal ions from aqueous solutions using graphene oxide. *Dalton Trans.* **2013**, *42*, 5682–5689.
51. Miao, M.; Feng, J.; Jin, Q.; He, Y.; Liu, Y.; Du, Y.; Zhang, N.; Li, D. Hybrid Ni–Al Layered Double Hydroxide/Graphene Composite Supported Gold Nanoparticles for Aerobic Selective Oxidation of Benzyl Alcohol. *RSC Adv.* **2015**, *5*, 36066–36074.
52. Cho, K.M.; Kim, K.H.; Park, K.; Kim, C.; Kim, S.; Al-Saggaf, A.; Gereige, I.; Jung, H.-T. Amine-functionalized graphene/CdS composite for photocatalytic reduction of CO₂. *ACS Catal.* **2017**, *7*, 7064–7069.
53. Zhou, X.; Wang, F.; Zhu, Y.; Liu, Z. Graphene modified LiFePO₄ cathode materials for high power lithiumion batteries. *J. Mater. Chem.* **2011**, *21*, 3353–3358.
54. Xie, W.; Zhang, F.; Wang, Z.; Yang, M.; Xia, J.; Gui, R.; Xia, Y. Facile preparation of PtPdPt/graphene nanocomposites with ultrahigh electrocatalytic performance for methanol oxidation. *J. Electroanal. Chem.* **2016**, *761*, 55–61.
55. Krishnamoorthy, K.; Veerapandian, M.; Mohan, R.; Kim, S.-J. Investigation of Raman and photoluminescence studies of reduced graphene oxide sheets. *Appl. Phys. A* **2012**, *106*, 501–506.
56. Johra, F.T.; Lee, J.-W.; Jung, W.-G. Facile and safe graphene preparation on solution based platform. *J. Ind. Eng. Chem.* **2014**, *20*, 2883–2887.
57. Kuniyil, M.; Kumar, J.; Adil, S.F.; Shaik, M.R.; Khan, M.; Assal, M.E.; Siddiqui, M.R.H.; Al-Warthan, A. One-pot synthesized Pd@ N-doped graphene: An efficient catalyst for Suzuki–Miyaura couplings. *Catalysts* **2019**, *9*, 469.
58. Parambath, V.B.; Nagar, R.; Ramaprabhu, S. Effect of Nitrogen Doping on Hydrogen Storage Capacity of Palladium Decorated Graphene. *Langmuir* **2012**, *28*, 7826–7833. [[CrossRef](#)]
59. Mahyari, M.; Shaabani, A. Graphene Oxide-Iron Phthalocyanine Catalyzed Aerobic Oxidation of Alcohols. *Appl. Catal. A* **2014**, *469*, 524–531.
60. Xu, C.; Zhang, L.; An, Y.; Wang, X.; Xu, G.; Chen, Y.; Dai, L. Promotional synergistic effect of Sn doping into a novel bimetallic Sn–W oxides/graphene catalyst for selective oxidation of alcohols using aqueous H₂O₂ without additives. *Appl. Catal. A* **2018**, *558*, 26–33.
61. Ramirez-Barria, C.S.; Isaacs, M.; Parlett, C.; Wilson, K.; Guerrero-Ruiz, A.; Rodríguez-Ramos, I. Ru nanoparticles supported on N-doped reduced graphene oxide as valuable catalyst for the selective aerobic oxidation of benzyl alcohol. *Catal. Today* **2019**, *357*, 8–14.
62. Yu, X.; Huo, Y.; Yang, J.; Chang, S.; Ma, Y.; Huang, W. Reduced Graphene Oxide Supported au Nanoparticles as an Efficient Catalyst for Aerobic Oxidation of Benzyl Alcohol. *Appl. Surf. Sci.* **2013**, *280*, 450–455.
63. Xie, X.; Long, J.; Xu, J.; Chen, L.; Wang, Y.; Zhang, Z.; Wang, X. Nitrogen-doped graphene stabilized gold nanoparticles for aerobic selective oxidation of benzylic alcohols. *RSC Adv.* **2012**, *2*, 12438–12446.
64. Hu, Z.; Zhao, Y.; Liu, J.; Wang, J.; Zhang, B.; Xiang, X. Ultrafine MnO₂ nanoparticles decorated on graphene oxide as a highly efficient and recyclable catalyst for aerobic oxidation of benzyl alcohol. *J. Colloid Interface Sci.* **2016**, *483*, 26–33.
65. Cai, M.; Li, J.; Wang, X.; Zhang, M.; Fang, Y.; An, Y.; Chen, Y.; Dai, L. Zn-doped W/aluminium oxide catalyst: Efficient strategy towards sustainable oxidation of alcohols. *Mol. Catal.* **2020**, *494*, 111114.
66. Hosseini-Sarvari, M.; Ataee-Kachouei, T.; Moeini, F. A novel and active catalyst Ag/ZnO for oxidant-free dehydrogenation of alcohols. *Mater. Res. Bull.* **2015**, *72*, 98–105.
67. Wu, Y.; Yu, H.; Wang, H.; Peng, F. Controllable synthesis and catalytic performance of graphene-supported metal oxide nanoparticles. *Chin. J. Catal.* **2014**, *35*, 952–959.
68. Jha, A.; Mhamane, D.; Suryawanshi, A.; Joshi, S.M.; Shaikh, P.; Biradar, N.; Ogale, S.; Rode, C.V. Triple nanocomposites of CoMn₂O₄, Co₃O₄ and reduced graphene oxide for oxidation of aromatic alcohols. *Catal. Sci. Technol.* **2014**, *4*, 1771–1778.
69. Wu, S.; He, Q.; Zhou, C.; Qi, X.; Huang, X.; Yin, Z.; Yang, Y.; Zhang, H. Synthesis of Fe₃O₄ and Pt nanoparticles on reduced graphene oxide and their use as a recyclable catalyst. *Nanoscale* **2012**, *4*, 2478–2483.
70. Yang, X.; Wu, S.; Hu, J.; Fu, X.; Peng, L.; Kan, Q.; Huo, Q.; Guan, J. Highly efficient N-doped magnetic cobalt-graphene composite for selective oxidation of benzyl alcohol. *Catal. Commun.* **2016**, *87*, 90–93.
71. Zheng, W.; Wu, M.; Yang, C.; Chen, Y.; Tan, R.; Yin, D. Alcohols selective oxidation with H₂O₂ catalyzed by robust heteropolyanions intercalated in ionic liquid-functionalized graphene oxide. *Mater. Chem. Phys.* **2020**, *256*, 123681.

-
72. Assal, M.E.; Shaik, M.R.; Kuniyil, M.; Khan, M.; Al-Warthan, A.; Alharthi, A.I.; Varala, R.; Siddiqui, M.R.H.; Adil, S.F. Ag₂O nanoparticles/MnCO₃–MnO₂ or–Mn₂O₃/highly reduced graphene oxide composites as an efficient and recyclable oxidation catalyst. *Arab. J. Chem.* **2018**, *12*, 54–68.
 73. Geng, L.; Wu, S.; Zou, Y.; Jia, M.; Zhang, W.; Yan, W.; Liu, G. Correlation between the microstructures of graphite oxides and their catalytic behaviors in air oxidation of benzyl alcohol. *J. Colloid Interface Sci.* **2014**, *421*, 71–77.
 74. Wu, G.; Wang, X.; Guan, N.; Li, L. Palladium on graphene as efficient catalyst for solvent-free aerobic oxidation of aromatic alcohols: Role of graphene support. *Appl. Catal. B Environ.* **2013**, *136*, 177–185.
 75. Feng, X.; Lv, P.; Sun, W.; Han, X.; Gao, L.; Zheng, G. Reduced graphene oxide-supported Cu nanoparticles for the selective oxidation of benzyl alcohol to aldehyde with molecular oxygen. *Catal. Commun.* **2017**, *99*, 105–109.
 76. Hasannia, S.; Yadollahi, B. Zn–Al LDH nanostructures pillared by Fe substituted Keggin type polyoxometalate: Synthesis, characterization and catalytic effect in green oxidation of alcohols. *Polyhedron* **2015**, *99*, 260–265.
 77. Hummers, W.S., Jr.; Offeman, R.E. Preparation of graphitic oxide. *J. Am. Chem. Soc.* **1958**, *80*, 1339.